www.czasopisma.pan.pl PAN www.journals.pan.pl
Chemical and Process Engineering 2018, 39 (4), 411–426
DOI: 10.24425/122960

MODELLING OF ERYTHROCYTE BEHAVIOUR IN BLOOD CAPILLARIES BY STRUCTURAL MODEL COMBINED WITH LATTICE-BOLTZMANN APPROACH

Rafał Przekop*, Igor Majewski, Arkadiusz Moskal

Faculty of Chemical and Process Engineering, Warsaw University of Technology, ul. Waryńskiego 1, 00-645 Warszawa, Poland

Dedicated to Professor Andrzej Burghardt on the occasion of his 90th birthday

A microstructural model of Red Blood Cell (RBC) behaviour was proposed. The erythrocyte is treated as a viscoelastic object, which is denoted by a network of virtual particles connected by elastic springs and dampers (Kelvin-Voigt model). The RBC is submerged in plasma modelled by lattice Boltzmann fluid. Fluid – structure interactions are taken into account. The simulations of RBC behaviour during flow in a microchannel and wall impact were performed. The results of RBC deformation during the flow are in good agreement with experimental data. The calculations of erythrocyte disaggregation from the capillary surface show the impact of RBC structure stiffness on the process.

Keywords: Red Blood Cells, Kelvin-Voigt model, lattice-Boltzmann

1. INTRODUCTION

Blood is a suspension of morphotic elements (erythrocytes, leukocytes and thrombocytes) in plasma. Morphotic elements constitute 40–45% of blood volume. The volume fraction of morphotic elements is called haematocrit and strongly influences the rheological properties of blood. Plasma is water with dissolved organic and inorganic compounds such as proteins, mainly albumin, globulin and fibrinogen and ions (Na^+, K^+, Cl^-). Plasma protects environmental stability of blood – pH, temperature, chemical composition and suspensions of cells.

Simulation of the blood flow may play an important role in diagnostic of several diseases caused by pathological changes in the mechanical properties of cells. In malaria or cancer, despite different source of the diseases, the changing of mechanical behaviour of living cells is reported. The disease progression is often accompanied by the changes in the mechanical properties of cells, such as a major change of elasticity modulus. Healthy Red Blood Cells (RBCs) are able to deform and be transported in tiny capillaries to deliver oxygen to various parts of the body but RBCs infected by protozoan *Plasmodium falciparum* loose these abilities, became stiff (Suresh, 2006) and may block the capillaries and disrupt the blood flow, leading to death.

The number of RBCs in 1 mm^3 of blood is typically in the range of 4.5–5.9 million. Erythrocytes do not have the nucleus or cytoplasmic cellular organelles. RBCs are shaped as biconcave discs which leads

* Corresponding author, e-mail: rafal.przekop@pw.edu.pl

to higher specific surface area in comparison with the sphere and allows to intensify gas exchange. The typical value of erythrocyte diameter is 6.9–9.0 μm, with the mean value of 7.5 μm. The surface of the RBC is equal to 120 μm^2. Philips et al. (2012) have estimated erythrocyte's mass and volume as 27.2 pg and 100.7 μm^3, respectively. This gives specific surface of the RBC equal approximately to 1.19 m^2/m^3, while for the sphere of similar diameter it is around 0.85.

Due to the high value of hematocrit, blood should be considered as a multiphase system. In the last decade interesting alternative approaches to solving Navier-Stokes equation were developed for multiphase flows. Lattice-Boltzmann method will be discussed later in more detail. Other models may be based on the formalism of thermodynamically compatible hyperbolic systems (Romenski et al., 2007; Zeidan, 2011; Zeidan, 2016; Zeidan et al., 2007). This approach recently became a base to formulate a model of viscous fluids, which can be also used for irreversible deformation of solids (Peshkov and Romenski, 2016).

In this study erythrocyte is treated as a viscoelastic object, which is denoted by a network of virtual particles connected by elastic springs and dampers. The modelled RBC is submerged in plasma modelled by the lattice Boltzmann fluid, so fluid – structure interactions are incorporated. The aim of this work was to check how elasticity of RBCs could influence their flow and interactions with blood capillary walls.

2. ERYTHROCYTE STRUCTURE, SHAPE AND PROPERTIES

Erythrocyte cell membrane consist of three layers:

- glycocalyx, the outer layer, built mainly of carbohydrates (galactose, glucose, glucosamine) connected with proteins and lipids of the outer lipid layer. Sugar residues are used to recognise the cells.
- lipid bilayer – forms the main layer structure. It makes up to 60% of cell membrane mass. Its thickness is approximately 7.5 nm. It contains, aside of lipids, many proteins. The mass ratio of lipids to proteins is close to one, but the number of lipid cells is much higher.
- protein scaffold (cytoskeleton) – is a mechanical support for a lipid membrane.

The key layer influencing the geometry of RBS is the lipid one. It can be described by 'liquid mosaic' model proposed by Singer and Nicolson (1972). According to this theory, biological membrane is built of a liquid bilayer of lipids and freely immersed proteins. Stiffness of such structure depends on temperature and the length of carbohydrate chains forming lipids. Additionally, the membrane has an asymmetrical structure and dynamic character. Lipids and proteins can perform rotational or translational moves or jump between the outer and inner layer (flip-flop movement). The bilayer structure of membrane is determined by amphipathic properties of lipids (the molecules have a hydrophilic head and a hydrophobic chain). Suspended in water environment, they spontaneously form a bilayer or spherical micelles.

There are three main groups of membrane lipids:

- phospholipids – the main lipid component of membranes. According to the group attached to phosphoric acid they are divided into amino phospholipids (e.g. phosphatidylserine, phosphatidylethanolamine) present mainly on the inner side of membrane and cholino ones (e.g. lecithin, sphingomyelin) occurring on the outer side.
- cholesterol – is distributed evenly in both layers. It stabilises the structure of membrane and keeps the liquidity of the membrane constant in lower temperatures.
- glycolipids – built of lipid molecule (sphingosine with a fatty acid) with sugar one (e.g. galactose) attached. They occur in the outer part exclusively.

The ratio between the lipid components in membrane influences the shape and mechanical properties of erythrocytes. The change of cholesterol to phospholipids or sphingomyelin to lecithin ratios leads to

stomatocyte (cells take an elongated shape) or echinocyte (cells have many, evenly distributed projections). The stiffness of the bilayer changes. A stiffer cell loses the ability to multiple strains occurring during the flow through blood capillaries. The main reason of deterioration of elastic properties is overabundance of cholesterol, sphingomyelin or phosphatidylethanolamine in the membrane structure.

The cytoskeleton is built of fibrous structured proteins forming the net. The thickness of the net is in the range of 40–90 nm (Lux, 2016). One of its tasks is keeping the ability to deform. Main proteins forming the scaffold are spectrins (α and β), ankyrin, actin and 4.1R. The key component is a spectrin forming elastic chains connected in a hexagonal net (containing other proteins in nodes). The deficiency of spectrin chains may lead to abnormalities in the net structure and loss of biconcave disc shape of the RBC (Ciana et al., 2011).

Human erythrocytes, free of the stresses, have the regular shape of biconcave discs. Their volume and shape depends on the osmotic pressure between the cell interior and the solution. In hypotonic solutions water is transported inside the cell and the RBC takes the spherical shape. Too high inflow of water may cause the burst of the cell membrane. In hypertonic environment the cell loses water.

The first geometrical model of mammal erythrocytes was proposed by Funaki (1955). The main assumptions were:

- RBC during the flow through both, large blood vessels and capillaries must minimise the drag;
- RBC have the negative charge and thus can be considered as a charged body;
- the shape of RBC should maximise gas exchange.

As a result the description of erythrocyte contour by Cassini oval was proposed. In polar coordinate system it takes the form:

$$r^4 + 2a^2r^2\cos\theta + a^4 = c^4 \tag{1}$$

while in Cartesian one:

$$\left(x^2 + y^2 + a^2\right)^2 - 4a^2x^2 = c^4 \tag{2}$$

where a, c are oval parameters, that can be related to sections p, q and L lengths (Fig. 1) by

$$L = 2c \tag{3}$$

$$pq = a^2 \tag{4}$$

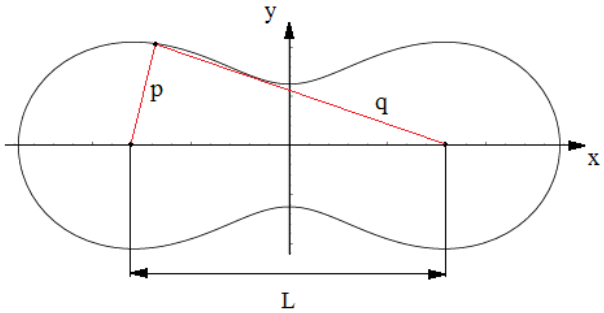

Fig. 1. Erythrocyte described by Cassini equation

The empirical equation of RBC shape was derived by Fung and Evans (1972):

$$h = \pm R_0\sqrt{1 - \left(\frac{r}{R_0}\right)^2}\left[C_0 + C_2\left(\frac{r}{R_0}\right)^2 + C_4\left(\frac{r}{R_0}\right)^4\right] \tag{5}$$

where h is erythrocyte's thickness as a function radius, r, R_0 is RBC's radius and C_i's are constant depending on solution osmolarity. For isotonic solution $R_0 = 3.91$ μm, $C_0 = 0.207161$ μm, $C_2 = 2.002558$ μm and $C_4 = -1.122762$ μm.

Another approach was presented by Deuling and Helfrich (1976). The authors have used the theory of elastic curves with foundations in description of liquid crystals, where bending energy per unit surface of membrane, g_c, is given by:

$$g_c = 0.5k_c\,(c_1 + c_2 - c_0)^2 + 0.5\bar{k}_c c_1 c_2 \tag{6}$$

Deuling and Helfrich (1976) have reported very good agreement of their model with the experimental findings of Fung and Evans (1972).

The crucial property in oxygen delivery to the cells are biomechanical properties of the erythrocytes, namely the ability for reversible deformation and to squeeze through blood capillaries with a size smaller than theirs. RBC's pliability depends on:

- ratio of surface to volume;
- viscosity of cytoplasm filling the cell interior;
- viscoelastic properties of cell membrane.

From the classical mechanics theory point of view, RBCs are viscoelastic biomaterials in which the properties of elastic (accumulating energy) and viscous (dissipating energy) body occur simultaneously.

As cytoplasm is a water solution, one can assume that a cell membrane is responsible for elastic properties of the erythrocyte. By assumption that, regardless of the multilayer and inhomogeneous structure, membrane can be treated as a continuous medium, pliability of membrane can be described by three modules (Fig. 2):

- area expansion modulus;
- shear modulus;
- bending modulus.

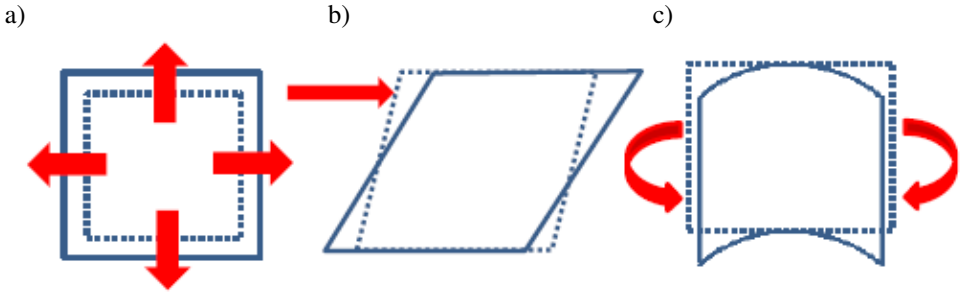

Fig. 2. Schematic presentation of deformations described by: a) area expansion modulus, b) shear modulus and c) bending modulus

The area expansion modulus, K, describes accumulation of energy during isotropic extension or squeezing a two-dimensional membrane.

$$T_t = K\frac{\Delta A}{A_0} \tag{7}$$

The value of area expansion modulus was estimated for the lipid bilayer by Rawicz et al. (2000) as equal to 300 μN/m. For the whole membrane the values depend on the experimental technique. Evans (1983) has used a micropipette aspiration technique (Evans and La Celle, 1975) and reported a value area expansion modulus ranging from 300–500 μN/m, while Gov et al. (2003) and Betz et al. (2009) using dynamic membrane fluctuations method estimated this modulus to be equal 10–100 μN/m. The value of the area expansion modulus decreases with increasing temperature (Waugh and Evans, 1979).

Shear modulus, μ, represents the accumulation of energy during the membrane deformation with constant surface:

$$T_s = \frac{\mu}{2}\left(\lambda^2 - \lambda^{-2}\right) \tag{8}$$

where T_s and λ are the shear force and the ratio of length after deformation to initial one, respectively (Evans, 1973).

The part of membrane responsible for non-zero value of shear modulus is the protein scaffold ($\mu = 0$ for liquid lipid layer). The value of shear modulus measured by the micropipette aspiration technique was reported to be from the range of 6–10 μN/m. The value of modulus decreases with increasing temperature (Waugh and Evans, 1979).

Bending modulus, B, describes the energy necessary for deformation of the membrane from its basic curvature to the shape of other curvatures.

$$M = B\left(C_1 + C_2 - C_3\right) \tag{9}$$

Bending modulus value depends on the chemical composition of lipid bilayer. Evans (1983) has estimated it, using the micropipette aspiration technique, to be equal 1.8×10^{-9} Nm. Nash and Meiselman (1985) have reported that there is no important effect of temperature on the bending modulus value.

The viscous properties of erythrocyte result from the presence of cytosol and cell membrane properties. Cytosol is a suspension composed of water (around 50%), organic (proteins, lipids, carbohydrates) and inorganic (mainly salts) compounds. Park et al. (2011) have estimated the value of cytosol viscosity to be equal approximately to 5 mPa·s. The increase of osmolarity results in the increase of cytosol viscosity. However, Evans and Hochmuth (1976) have proved that, during the return to the original shape after the deformation, the viscosity of cell membrane plays a crucial role in energy dissipation. To estimate the surface viscosity of membrane, the diffusivity of proteins anchored in the membrane may be used (Saffmann and Delbruck, 1975). The results were in the range of $0.5 - 14 \times 10^{-9}$ Ns/m.

3. ERYTHROCYTE MECHANICAL MODELS

The mechanical models of RBCs may be divided into two main groups, continuous and structural ones. In continuous approach cell membrane is discretised using shell or membrane type elements for finite element (Chee et al., 2008; Dao et al., 2003; Mills et al., 2004; Yoon and You, 2016) or boundary element analysis (Pozrikidis, 2003). Strain energy density functions have been adopted for modelling elasticity of erythrocyte membrane (Cordasco and Bagchi, 2014; Peng et al., 2011; Tan et al., 2010). The orders of functions which characterise the elastic behaviour of cell membrane range from the first to third order. High order models such as the Yeoh model and the reduced polynomial model have rarely been employed (Chee et al., 2008; Mills et al., 2004).

A particle-based method in general refers to the class of mesh-free methods that employ a set of finite number of discrete particles to represent the state of a flow system and to record the evolution of the system (Liu and Liu, 2003). Compared with mesh-based methods, it is founded on a set of arbitrarily distributed particles and thus is attractive in dealing with complex structures. The particle-based methods may be divided into two main groups: Dissipative Particle Dynamics (mesoscopic), Smoothed Particle Dynamics (macroscopic).

Dissipative Particle Dynamics (DPD) was originally designed as a mesoscopic stochastic simulation technique by Hoogerbrugge and Koelman (1992). In RBC modelling, different DPD particles are employed to

distinguish different components in the computational domain. All these particles move in accordance with the Newton's second law of motion (Ye et al., 2014). Currently, there are two types of widely-used RBC models, shell-based and spring-based membrane models (Fedosov et al., 2010; Li et al., 2005; Pozrikidis, 2001). The former shell-based model assumes the RBC membrane as a highly deformable shell without thickness, while the latter spring-based model treats the RBC membrane as a triangular network connected by elastic or viscoelastic springs.

Smoothed Particle Hydrodynamics (SPH) is a macroscopic particle-based method proposed by Gingold and Monaghan (1977) and Lucy (1977). SPH starts with the Navier–Stokes equations, employs a continuous Lagrangian interpolation using a kernel function (delta sequence) to discretise the whole computational domain into a set of particles (Violeau, 2012). Each particle has a spatial distance, called the smoothing length, over which its physical properties are given by the kernel function. SPH particle discretisation for a RBC also leads to different types of particles to distinguish different components in computational domain, in the same manner as in the DPD method. All particles move according to Newton's second law (Hosseini and Feng, 2009). SPH forces result directly from discretising the Navier–Stokes equations (assuming a Newtonian fluid), and hence it has specific physical parameters like viscosity with clear physical scales. DPD forces are arbitrarily chosen conservative, dissipative and random forces. In SPH, the physical field quantities (like density, and velocity) are obtained directly after each solution time step; in DPD, a further average needs to be processed to obtain filed quantities.

4. SPRING-BASED MODEL

In this study we propose a two-dimensional structural model of RBC. The erythrocyte contour is described by 20 particles and cytosol by additional 3 (Fig. 3). The initial position of membrane particles is described by Fung-Evans equation (Eq. (5)) with constants for isotonic solution.

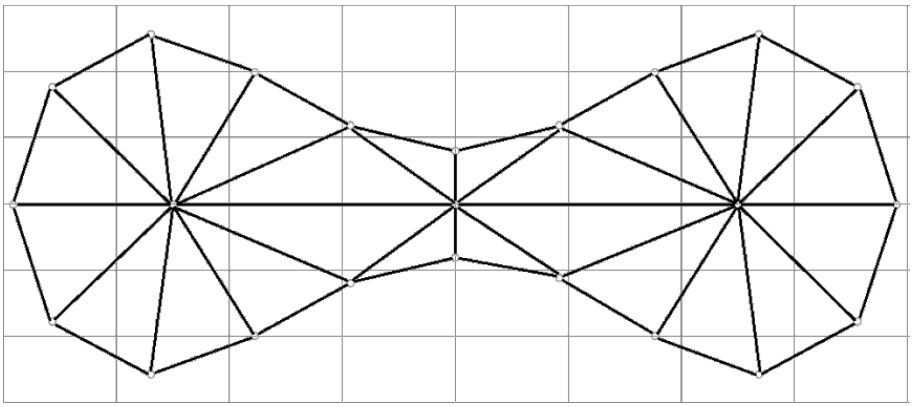

Fig. 3. Scheme of RBC geometry model

The interactions between particles are described by viscoelastic Voigt-Kelvin model. The Voigt-Kelvin model consists of a spring and a damper connected in parallel (Fig. 4). The deformation of the system, ε is equal to the deformations of each element:

$$\varepsilon = \varepsilon_s = \varepsilon_d \tag{10}$$

The total stress, σ, is a sum of stresses on both elements

$$\sigma = \sigma_s + \sigma_d \tag{11}$$

Thus, the relation between stress and deformation has the form:

$$\sigma = k_s \varepsilon(t) + \eta \frac{d\varepsilon(t)}{dt} \tag{12}$$

where η is dynamic viscosity.

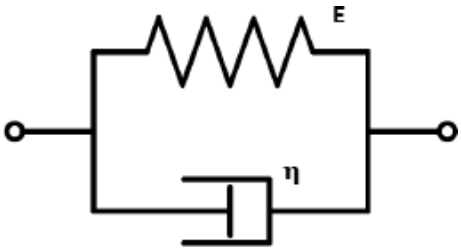

Fig. 4. The Kelving-Voigt body model

By applying constant stress, σ_0, one can obtain the creeping function:

$$\varepsilon(t) = \frac{\sigma_0}{k_s}\left[1 - \exp\left(-\frac{k_s}{\eta}t\right)\right] \tag{13}$$

The specific quantity resulting from material properties is relaxation time, τ, expressed as viscosity and Young's modulus ratio.

$$\tau = \frac{\eta}{k_s} \tag{14}$$

It can be interpreted as a time after which the stress decreases e times.

Converting Eq. (5) for a two-dimensional case one can write:

$$F_{K-V,i}(t) = K_s \varepsilon(t) + A_v \frac{d\varepsilon(t)}{dt} \tag{15}$$

The time derivative of linear deformation is approximated by finite difference

$$\frac{d\varepsilon}{dt} = \frac{\varepsilon(t+\Delta t) - \varepsilon(t)}{\Delta t} \tag{16}$$

The RBC is affected by fluid through drag force. Its value may be computed from modified Stokes law, as one can assume the laminar flow in blood capillaries. Membrane model consist of N particles connected. We assume that fluid interacts only with surface particles.

$$F_{D,i} = 3\pi\eta d_p \left(U_i - u_f\right) \tag{17}$$

The value of d_p was estimated by dividing the RBC contour length by the number of particles forming the membrane.

To model Plasma Flow the lattice-Boltzmann algorithm was used. It allows to apply easily non-steady state boundary conditions and update the system geometry related to displacement and deformation of RBCs.

Complete information on the statistical description of a gas at, or near, thermal equilibrium is assumed to be contained in the one-particle phase-space distribution function $f(x,t,\Gamma)$ for the atomic constituents of the system. The variables x and t are the space and time coordinates of the atoms and Γ stands for all other phase-space coordinates e.g. momentum, momentum flux.

For the isolated gas with collisions the Liouville theorem is modified to the form:

$$\partial_f t + u\nabla f = \Omega(f) \tag{18}$$

where, $\Omega(f)$ is a function that models the rate of changes of distribution function.

The form of $\Omega(f)$ was proposed by Boltzmann (1995). Since collisions preserve conservation laws, the equations describing the macro dynamics of the system can be derived by integration of Boltzmann equation. To build the cellular-space picture with dynamics of the collective motion predicted by Navier-Stokes equation, a lattice on which particles move, collision rules and other restrictions characteristic for a chosen model should be defined. In this work a 2-dimensional lattice with 9 allowed directions of movement, usually referred as D2Q9 was used (Fig. 5).

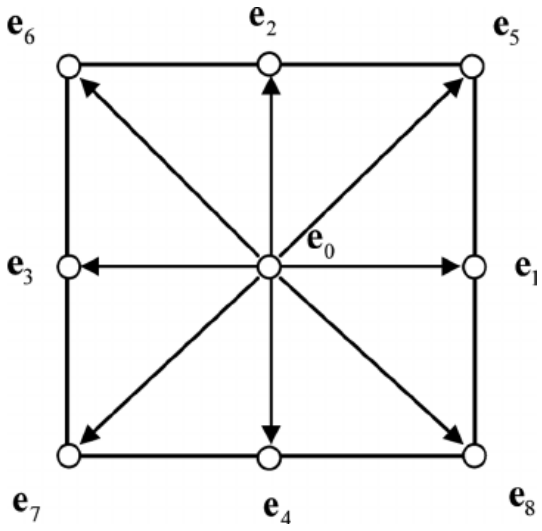

Fig. 5. D2Q9 lattice geometry

The evolution of the system is described by the expression:

$$f(\bar{x}+e_i,\bar{t}+1)-f(\bar{x},\bar{t})=\Omega_i(f) \tag{19}$$

The outcome of collision can be approximated by assuming that the momentum of interacting particles will be redistributed at some constant rate toward an equilibrium distribution f_i^{eq} (Qian et al., 1992). This simplification is called single-time-relaxation approximation and can be expressed by the equation:

$$\Omega_i=\frac{1}{\bar{\tau}}\left[f_{i^{eq}}(\bar{x},\bar{t})-f_i(\bar{x},\bar{t})\right] \tag{20}$$

In the single-time-relaxation approximation, the momentum distribution at each lattice site is forced toward the equilibrium distribution at each time step. In the absence of external forces, the equilibrium distribution of a state with zero net momentum is just equal to momentum in each direction. The rate of change toward equilibrium is the inverse of relaxation time, and is chosen to produce the desired value of fluid viscosity.

$$\overline{\eta}=\frac{\overline{c}_{s^2}}{2}(2\overline{\tau}-1) \tag{21}$$

The equilibrium distribution f_i^{eq} is given as follows:

$$f_i^{eq}=\overline{\rho}\alpha_i\left(1+\frac{e_i\overline{u}}{\overline{c}_{s^2}}+\frac{1}{2}\left(\frac{e_i\overline{u}}{\overline{c}_{s^2}}\right)^2-\frac{\overline{u}^2}{\overline{c}_{s^2}}\right) \tag{22}$$

where a_i are the model dependent constants. The values of parameters in Eq. (22) depend on the lattice geometry.

5. RESULTS AND DISCUSSION

To verify the model, the effect of constants A_s and K_v (Eq. (15)) on the RBC behaviour during the wall impact with velocity of 1000 μm/s, which is a typical value of flow velocity in blood capillaries, was studied. As a parameter to measure the deformation the ratio of maximal, $P_{\max}$, and minimal, $P_{\min}$, erythorcyte surface to the stationary one, P_0, may be applied:

$$E_{\max} = \frac{P_{\max}}{P_0} \tag{23}$$

$$E_{\min} = \frac{P_{\min}}{P_0} \tag{24}$$

The results are presented in Figs. 6–8.

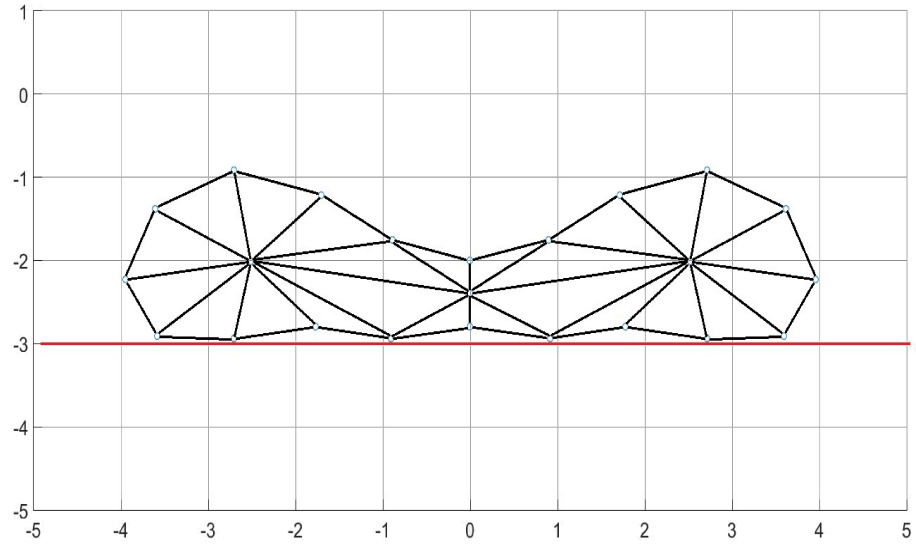

Fig. 6. Picture of RBC during wall impaction, $K_s = 2.5 \times 10^5$ N, A_v =10 Ns

The obtained results confirm the model assumptions. The increase of damper viscosity or elasticity parameter leads to increase of RBC stiffness. The deformation tends to unity. $E_{\min}$ was assumed to be the key parameter as it describes cell compression ability.

The next step was to choose the parameters K_s and A_v that reproduce the behaviour of the real RBC. Tsukada et. al (2001) have experimentally studied erythrocyte deformation in a microchannel of 9.3 μm diameter flow.

For the fluid flow the plug flow with assumed mean velocity and equilibrium distribution was applied at the channel inlet. At the outlet and channel walls no-stress and bounce-back conditions, respectively, were applied The boundary conditions on the surface of a moving object (RBC) were applied according to the method proposed by Lallemand and Luo (2003), which was a simple extension of the treatment for a curved boundary proposed by Bouzidi et al. (2002), which is a combination of standard bounce-back condition on the solid level and interpolations.

When a grid point moves out of the non-fluid region into the fluid region to become a fluid node, one must specify some number of unknown distribution functions on this node. We use a second order extrapolation to compute the unknown distribution functions along the direction of a chosen discrete velocity e_i which maximises the quantity of $\mathbf{n}e_i$, where $\mathbf{n}$ is the out-normal vector of the wall at the point, through which the

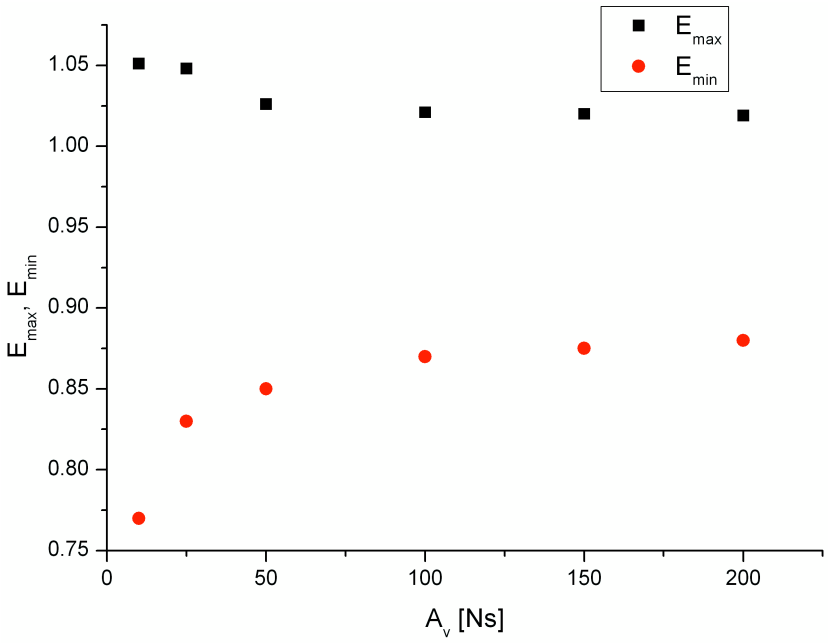

Fig. 7. $E_{\max}$ and $E_{\min}$ as a function of parameter A_v for the constant value of parameter $K_s = 5 \times 10^5$ N

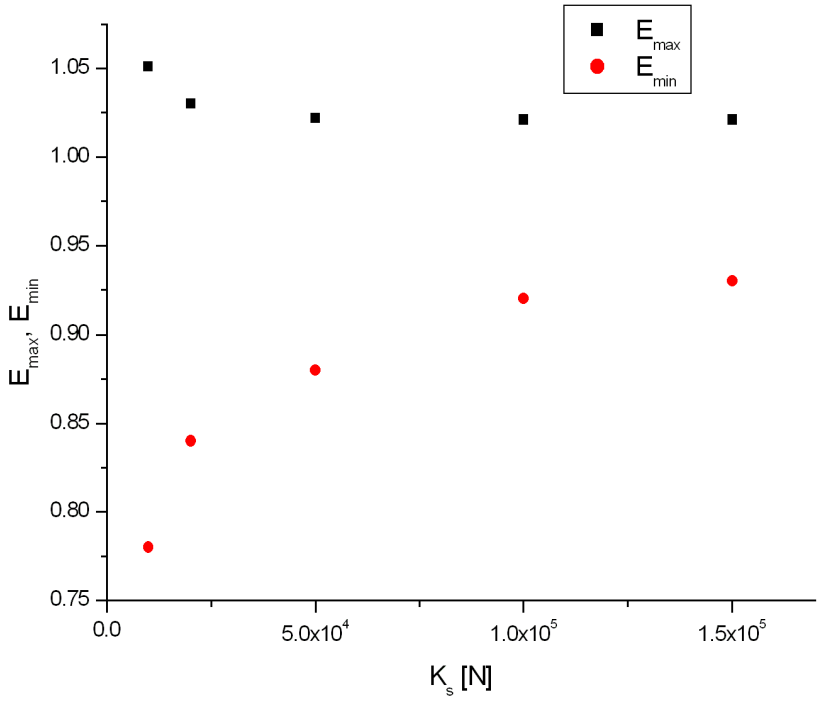

Fig. 8. $E_{\max}$ and $E_{\min}$ as a function of parameter K_s for the constant value of parameter $A_v = 100$ Ns

node moves to the fluid region. The deformation was described by deformation index (Fig. 9):

$$DI = \frac{L}{D} \tag{25}$$

At this point, we have assumed that model constants for membrane and cytosol particles are different, since they better reproduce the real biomechanics of RBC. By trial and error method the values of model constants were estimated for the membrane: $K_{s,mem} = 1.58 \times 10^6$ N, $A_{v,mem} = 52.6$ Ns and for cytosol: $K_{s,cyt} = 2.38 \times 10^5$ N, $A_{v,cyt} = 11.3$ Ns.

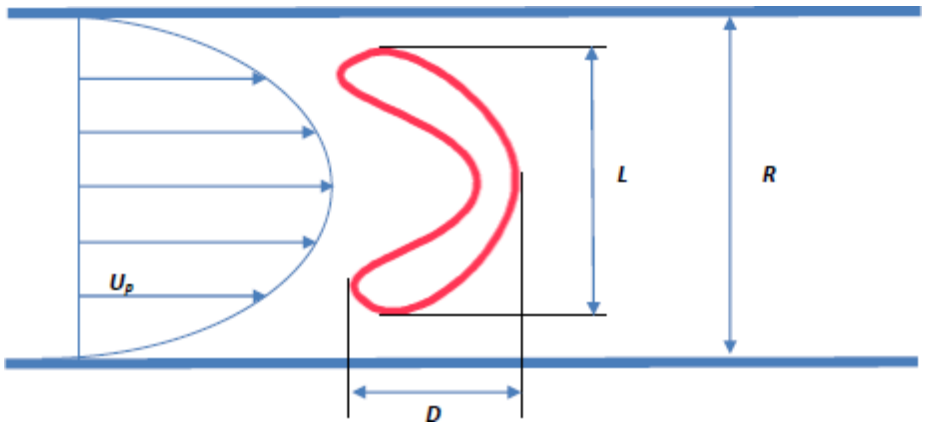

Fig. 9. Definition of Deformation Index (*DI*)

The picture of erythrocyte flowing with the velocity of 0.1 mm/s and comparison of experimental and theoretical data are presented in Figs. 10 and 11, respectively.

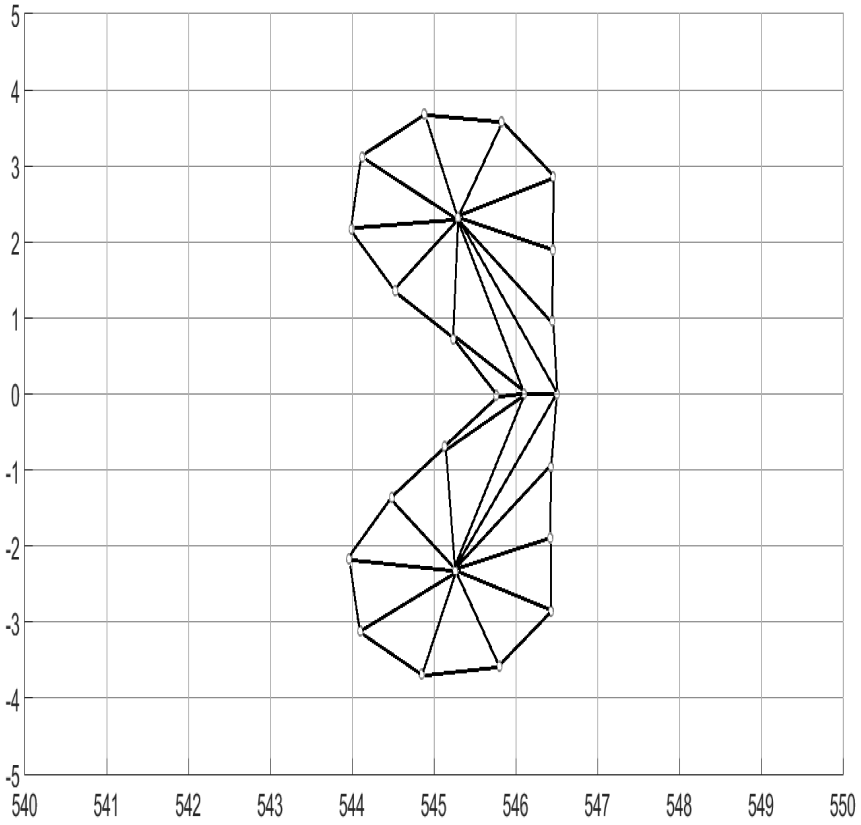

Fig. 10. Picture of RBC during the flow through microchannel

The last investigated problem was detachment of RBC from the solid wall. The erythrocyte was initially attached to the capillary with the distance between surfaces equal to $L_0 = 10$ nm (Fig. 12).

The detachment was assumed to occur when the length of the connection exceeded $L_{gr} = 20$ nm (Yoon and You, 2016). The calculations of fluid velocity at which the detachment occurred, $u_{p,\max}$, were performed for 7 cases of RBC parameters, obtained to reproduce behaviour during flow through a capillary, 3 stiffened and 3 elastised (Table 1).

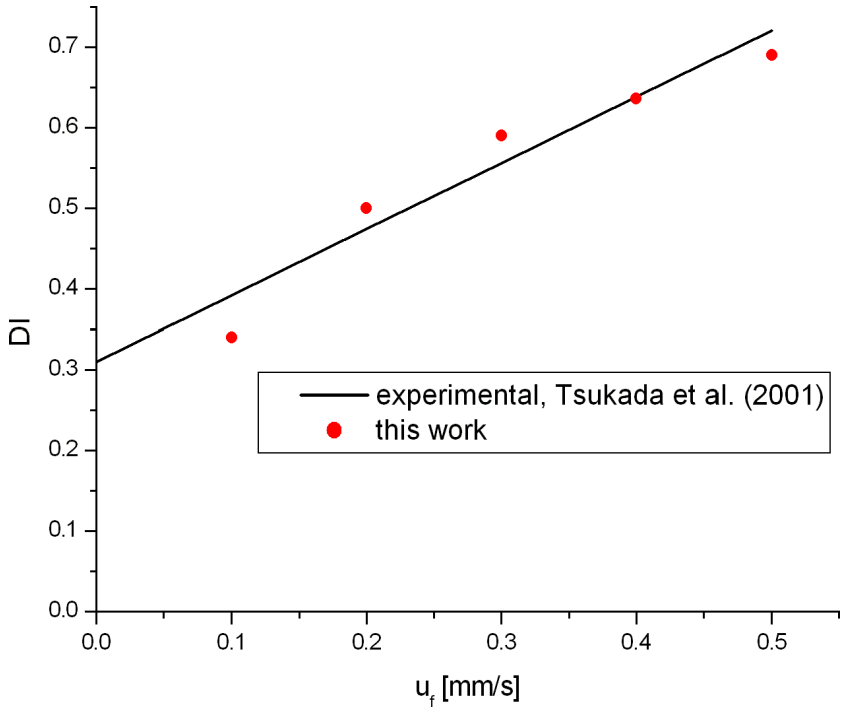

Fig. 11. Deformation Index as a function fluid flow velocity

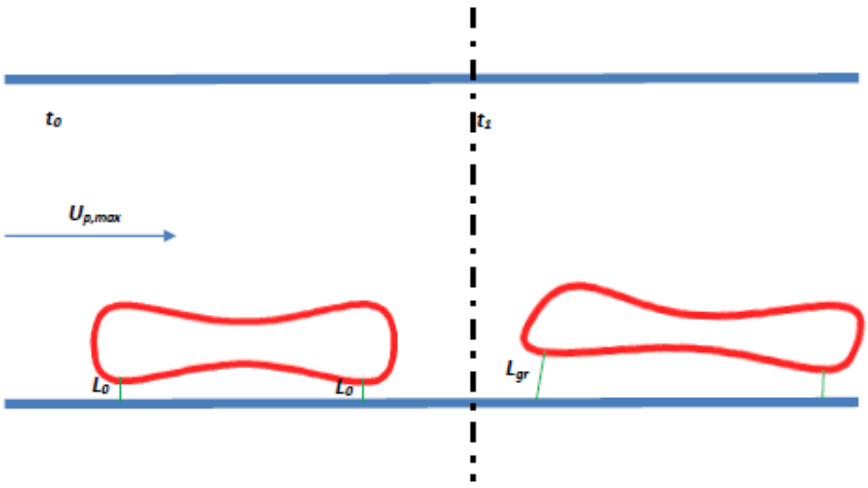

Fig. 12. Scheme of RBC detachment investigation

Table 1. Mechanical properties and velocity at which detachment occured

RBC	$K_{s,mem}$ [N]	$K_{s,cyt}$ [N]	$A_{v,mem}$ [Ns]	$A_{v,cyt}$ [Ns]	$u_{p,\max}$ [μm/s]
+10%	1.74×10^6	1.58×10^5	57.9	12.4	44.5
+5%	1.66×10^6	2.50×10^5	55.2	11.9	43.4
0	1.58×10^6	2.38×10^5	52.6	11.3	42.3
−5%	1.50×10^6	2.26×10^5	50.0	10.7	41.3
−10%	1.42×10^6	2.14×10^5	47.3	10.2	40.2
elastic	10^6	10^5	25	5	38.5
stiff	2×10^6	5×10^5	100	50	47.8

6. CONCLUSIONS

The results show that a simple structural, two-parameter model can satisfactorily describe the behaviour of RBCs. The results confirm that stiff erythrocytes have lower for susceptibility disaggregation from capillary surface. This behaviour is not caused by increase of contact area, but by the momentum transfer in the RBC structure. The next step of the research will be focused on predicting the rheological properties of blood directly from plasma – RBC interactions.

This work was supported by National Science Centre, Poland under Grant number UMO-2015/19/B/ST8/00599.
This work is a part of biomechanical research initiated at Faculty of Chemical and Process Engineering, Warsaw University of Technology by Professor Leon Gradoń.

SYMBOLS

a	oval parameter, m
A	membrane surface, m^2
A_0	initial membrane surface, m^2
A_v	viscous parameter, Ns
B	bending modulus, Nm
c	oval parameter, m
c_0	spontaneous curvature of membrane, m^{-1}
c_i	principle curvatures of membrane, m^{-1}
C_i	constants, –
$\overline{c}_s$	dimensionless sound speed, –
d_p	particle diameter, m
DI	deformation index, –
e	lattice spacing, –
$E_{\max}$	ratio of maximal erythrocyte surface to stationary one, –
$E_{\min}$	ratio of minimal erythrocyte surface to stationary one, –
f	distribution function, –
f^{eq}	equilibrium distribution function, –
F_D	drag force, N
F_{K-V}	Kelvin-Voigt force, N
g_c	bending energy per unit surface of membrane, Pa/m^2
h	erythrocyte thickness, m
K	area expansion modulus, N/m
K_s	stiffness parameter, N
k_c	Young's modulus, Pa
$\overline{k}_c$	Young's modulus for Gauss curvature, Pa
L	characteristic length, m
L_0	initial length of erythrocyte-wall connection, m
L_{gr}	breakup length of erythrocyte-wall connection, m
M	bending moment, Nm
p	characteristic length, m
P_0	stationary erythrocyte surface, m^2
$P_{\max}$	maximal erythrocyte surface, m^2
$P_{\min}$	minimal erythrocyte surface, m^2

q	characteristic length, m
r	radius, m
R_0	erythrocyte radius, m
t	time, s
$\bar{t}$	dimensionless time, –
T_s	shear force, N/m
T_t	extending force, N/m
U	particle velocity, m/s
$\bar{u}$	dimensionless velocity, –
$u_{p,\max}$	breakup velocity of erythrocyte-wall connection, m/s
u_f	fluid velocity, m/s
$\bar{x}$	dimensionless position, –

Subscripts

cyt	cytosol
mem	membrane

Greek

α_i	constants, –
ε	deformation, –
ε_d	damper deformation, –
ε_s	spring deformation, –
λ	ratio of length after deformation to initial one, –
μ	shear modulus, N/m
η	viscosity, Pas
$\bar{\eta}$	dimensionless viscosity, –
$\bar{\rho}$	dimensionless density, –
σ	stress, Pa
σ_d	damper stress, Pa
σ_s	spring stress, Pa
τ	relaxation time, s
$\bar{\tau}$	dimensionless relaxation time, –
Ω	collision operator, –

REFERENCES

Betz T., Lenz M., Joanny J.F., Sykes C., 2009. ATP-dependent mechanics of red blood cells. *PNAS*, 106, 15312–15317. DOI: 10.1073/pnas.0904614106.

Boltzmann L., 1995. *Lectures on Gas Theory*. Dover Publishing, New York, USA.

Bouzidi, M., Firdaouss, P., Lallemand, P., 2002. Momentum transfer of lattice-Boltzmann fluid with boundaries. *Phys. Fluids*, 13, 3452–3459. DOI: 10.1063/1.1399290.

Chee C.Y., Lee H.P., Lu C., 2008. Using 3D fluid-structure interaction model to analyse the biomechanical properties of erythrocyte. *Phys. Lett. A*, 372, 1357–1363. DOI: 10.1016/j.physleta.2007.09.067.

Ciana A., Achilli C., Bakluini C., Minetti G., 2011. On the association of lipid rafts to the spectrin skeleton in human erythrocytes. *Biochim. Biophys. Acta*, 1808, 183–190. DOI: 10.1016/j.bbamem.2010.08.019.

Cordasco D., Bagchi. P., 2014. Intermittency and synchronized motion of red blood cells dynamics in shear flow. *J. Fluid Mech.*, 759, 472–488. DOI: 10.1017/jfm.2014.587.

Dao M., Lim C.T., Suresh S., 2003. Mechanics of the human red blood cell deformed by optical tweezers. *J. Mech. Phys. Solids*, 51, 2259–2280. DOI: 10.1016/j.jmps.2003.09.019.

Deuling H.J., Helfrich W., 1976. The curvature elasticity of fluid membranes: A catalogue of vesicle shapes. *J. Phys.*, 37, 1335–1345. DOI: 10.1051/jphys:0197600370110133500.

Evans E.A., 1973. New membrane concept applied to the analysis of fluid-shear and micropipette-deformed red blood cells. *Biophys. J.*, 13, 941–954. DOI: 10.1016/S0006-3495(73)86036-9.

Evans E.A., 1983. Bending elastic modulus of red blood cell membrane derived from buckling instability in micropipette aspiration tests. *Biophys. J.*, 43, 27–30. DOI: 10.1016/S0006-3495(83)84319-7.

Evans E.A., Hochmuth R.M., 1976. Membrane viscoelasticity. *Biophys. J.*, 16, 1–11. DOI: 10.1016/S0006-3495 (76)85658-5.

Evans E.A., La Celle P.L., 1975. Intrinsic material properties of the erythrocyte membrane indicated by mechanical analysis of deformation. *Blood*, 45, 29–43.

Fedosov D.A., Caswell B., Karniadakis G.E., 2010. Systematic coarse-graining of spectrin-level red blood cells models. *Comput. Metods. Appl. Mech. Eng.*, 199, 1937–1948. DOI: 10.1016/j.cma.2010.02.001.

Funaki H., 1955. Contributions on the shapes of red blood corpuscles. *Jpn. J. Physiol.*, 5, 81–92. DOI: 10.2170/jjphysiol.5.81.

Fung Y.C., Evans E., 1972. Improved measurements of the erythrocyte geometry. *Microvasc. Res.*, 4, 335–347. DOI: 10.1016/0026-2862(72)90069-6.

Gingold R.A., Monaghan J.J., 1977. Smoothed particle hydrodynamics: theory and application to non-spherical stars. *Mon. Not. R. Astron. Soc.*, 181, 375–389. DOI: 10.1093/mnras/181.3.375.

Gov N., Zilman A.G., Safran S., 2003. Cytoskeleton confinement and tension of red blood cells membranes. *Phys. Rev. Lett.*, 90, 228101. DOI: 10.1103/PhysRevLett.90.228101.

Hoogerbrugge P.J., Koleman J.M.V.A., 1992. Simulating microscopic hydrodynamic phenomena with dissipative particle dynamics. *Europhys. Lett.*, 19, 155–160. DOI: 10.1209/0295-5075/19/3/001.

Hosseini S.M., Feng J.J., 2009. A particle-based model for the transport of erythrocytes in capillaries. *Chem. Eng. Sci.*, 64, 4488–4497. DOI: 10.1016/j.ces.2008.11.028.

Lallemand P., Luo L.S., 2003. Lattice Boltzmann method for moving boundaries. *J. Comput. Phys.*, 184, 406–421. DOI: 10.1016/S0021-9991(02)00022-0.

Li J., Dao M., Lim C.T., Suresh S., 2005. Spectrin-level modelling of the cytoskeleton and optical tweezers stretching of the erythrocyte. *Biophys. J.*, 88, 3707–3719. DOI: 10.1529/biophysj.104.047332.

Liu Y., Liu W.K., 2006. Rheology of red blood cells aggregation by computer simulation. *J. Comput. Phys.*, 220, 139–154. DOI: 10.1016/j.jcp.2006.05.010.

Lucy L.B., 1977. A numerical approach to the testing of fission hypothesis. *Astron. J.*, 82, 1013–1024. DOI: 10.1086/112164.

Lux S.E., 2016. Anatomy of the red cell membrane skeleton: unanswered questions. *Blood*, 127, 527–536. DOI: 10.1182/blood-2014-12-512772.

Mills J., Qie L., Dao M., Lim C., Shuresh S., 2004. Nonlinear elastic and viscoelastic deformation of the human red blood cell with optical tweezers. *Mol. Cell. Biomech.*, 1, 169–180. DOI: 10.3970/mcb.2004.001.169.

Nash G., Meiselman H.J., 1985. Alteration of red cell membrane viscoelasticity by heat treatment: effect on cell deformability and suspension viscosity. *Biorheology*, 22, 73–84. DOI: 10.3233/BIR-1985-22106.

Park Y., Best C.A., Kuriabova T., Henle M.L., Feld M.S., Levine A.J., Popescu G., 2011. Measurement of the nonlinear elasticity of red blood cell membranes. *Phys. Rev. E*, 83, 051925. DOI: 10.1103/PhysRevE.83.051925.

Peng Z.L., Asaro R.J., Zhu Q., 2011. Multiscale simulation of erythrocyte membrane. *Phys. Rev. E*, 81, 031904. DOI: 10.1103/PhysRevE.81. 031904.

Peshkov I., Romenski E., 2016. A hyperbolic model for viscous Newtonian fluids. *Continuum Mech. Thermodyn.*, 28, 85–104. DOI: 10.1007/s00161-014-0401-6.

Philips K.G., Jacques S.L., McCarthy O.J.T., 2012. Measurement of the single cell refractive index, dry mass, volume and density using a transillumination microscope. *Phys. Rev. Lett.*, 109, 118105. DOI: 1103/PhysRevLett. 109.118105.

Pozrikidis C., 2001. Effect of membrane bending stiffness on the deformation of capsules in simple shear flow. *J. Fluid Mech.*, 440, 269–291. DOI: 10.1017/S0022112001004657.

Pozrikidis C., 2003. Numerical simulation of the flow-inducted deformation of red blood cells. *Ann. Biomed. Eng.*, 31, 1194–1205. DOI: 19.1114/1.1617985.

Qian Y.H., d'Humieres D., Lallemand P., 1992. Lattice BGK model for Navier-Stokes equation. *Europhys. Lett.*, 17, 479–484. DOI: 10.1209/0295-5075/17/6/001.

Rawicz W., Olbrich K.C., McIntosh T., Needham D., Evans E.A., 2000. Effect of chain length and unsaturation on elasticity of lipid bilayers. *Biophys. J.*, 79, 328–339. DOI: 10.1016/S0006-3495(00)76295-3.

Romenski E., Resnyansky A.D., Toro E.F., 2007. Conservative hyperbolic formulation for compressible two-phase flow with different phase pressures and temperatures. *Quart. App. Math.*, 45, 259–279. DOI: 10.1090/qam/1409.

Saffman P., Delbruck M., 1975. Brownian motion in biological membranes. *Proc. Natl. Acad. Sci. USA*, 72, 3111–3113. DOI: 10.1073/pnas.72.8.3111.

Singer S.J., Nicolson G.L., 1972. The fluid mosaic model of the structure of cell membranes. *Science*, 175, 720–731. DOI: 10.1126/science.1975.4023.720.

Suresh S., 2006. Mechanical response of human red blood cells in health and disease: Some structure-property-function relationships. *J. Mater. Res.*, 21, 1871–1877. DOI: 10.1557/jmr.2006.0260.

Tan Y., Sun D., Huang W., 2010. Mechanical modelling of red blood cells during stretching. *J. Biomech. Eng.*, 132, 4001042. DOI: 10.1115/1.4001042.

Tsukada K., Sekizuka E., Oshio C., Minamitani H., 2001. Direct measurement of erythrocyte deformability in diabetes mellitus with a transparent microchannel capillary model and high-speed video camera system. *Microvasc. Res.*, 61, 231–239. DOI: 10.1006/mvre.2001.2307.

Violeau D., 2012. *Fluid mechanics and the SPH method: Theory and applications*. Oxford University Press, Oxford, UK.

Waugh R., Evans E.A., 1979. Thermoelasticity of red blood cell membrane. *Biophys. J.*, 26, 115–131. DOI: 10.1016/S0006-3495(79)85239-X.

Ye T., Phan-Thien N., Khoo B.C., Lim C.T., 2014. Numerical modelling of a healthy/malaria infected erythrocyte in shear flow using dissipative particle dynamics method. *J. Appl. Phys.*, 115, 224710. DOI: 10.1063/1.4879418.

Yoon D., You D., 2016. Continuum modelling of deformation and aggregation of red blood cells. *J. Biomech.*, 49, 2267–2279. DOI: 10.1016/j.biomech.2015.11.027.

Zeidan D., 2011. Numerical resolution for a compressible two-phase flow model based on the theory of thermodynamically compatible systems. *Appl. Math. Comp.*, 217, 5023–5040. DOI: 10.1016/j.amc.2010.07.053.

Zeidan D., 2016. Assessment of mixture two-phase flow equations for volcanic flows using Godunov-type methods. *Appl. Math. Comp.*, 272, 707–719. DOI: 10.1016/j.amc.2015.09.038.

Zeidan D., Romenski E., Slaouti A., Toro F., 2007. Numerical study of wave propagation in compressible two-phase flow. *Int. J. Numer. Meth. Fluids*, 54, 393–417. DOI: 10.1002/fld.1404.

Received 20 July 2018
Received in revised form 09 October 2018
Accepted 11 October 2018